The Influence of the Effect of Solute on the Thermodynamic Driving Force on Grain Refinement of Al Alloys

FENG WANG, ZHI-LIN LIU, DONG QIU, JOHN A. TAYLOR, MARK A. EASTON, and MING-XING ZHANG

Grain refinement is known to be strongly affected by the solute in cast alloys. Addition of some solute can reduce grain size considerably while others have a limited effect. This is usually attributed to the constitutional supercooling which is quantified by the growth restriction factor, Q. However, one factor that has not been considered is whether different solutes have differing effects on the thermodynamic driving force for solidification. This paper reveals that addition of solute reduces the driving force for solidification for a given undercooling, and that for a particular Q value, it is reduced more substantially when adding eutectic-forming solutes than peritectic-forming elements. Therefore, compared with the eutectic-forming solutes, addition of peritectic-forming solutes into Al alloys not only possesses a higher initial nucleation rate resulted from the larger thermodynamic driving force for solidification, but also promotes nucleation within the constitutionally supercooled zone during growth. As subsequent nucleation can occur at smaller constitutional supercoolings for peritectic-forming elements, a smaller grain size is thus produced. The very small constitutional supercooling required to trigger subsequent nucleation in alloys containing Ti is considered as a major contributor to its extraordinary grain refining efficiency in cast Al alloys even without the deliberate addition of inoculants.

I. INTRODUCTION

IN the commercial production of aluminum alloys, inoculation *i.e.*, adding alloying elements or/and nucleant particles, is commonly used to achieve fine, uniform, and equiaxed grains. This not only improves the properties of cast metals and facilitates the subsequent formability,[1,2] but also benefits the casting process through reducing cast defects, such as hot tears, segregation, and porosity. Over the last 60 years, grain refinement in cast Al alloys has been comprehensively studied.[1–8] Although there is still controversy over aspects of the grain refinement mechanism, it is now generally agreed that there are two essential contributions: numerous potent inoculants and sufficient effective solutes.[7–10] Inoculant particles that are able to trigger nucleation of α-Al at small undercooling promote grain refinement *via* enhanced heterogeneous nucleation.[3,6,11,12] The role of solute in grain refinement is generally attributed to the solute partitioning in the liquid ahead of the solid–liquid interface. Such segregation not only restricts the growth of solid but also generates a constitutionally supercooled zone in front of the growing solid, providing additional driving force to facilitate further subsequent nucleation within the constitutionally supercooled zone.[13–15] It should be noted that in the present work the nucleation that occurs within the constitutionally supercooled zone is called subsequent nucleation in order to distinguish the nucleation that is not associated with constitutional supercooling. StJohn and his co-workers[13,14,16] have recently developed the 'Interdependence Theory' to describe the role of constitutional supercooling zone in grain refinement. The overall effect of solute is quantified by the growth restriction factor/parameter $Q = \Sigma\ m \cdot (k - 1) \cdot c_i$, where m is the slope of liquidus, k the equilibrium partitioning coefficient, and c_i is the concentration of each element in the alloy.[15,17,18] Extensive studies, including experimental work[19–22] and analytical modeling,[13,14,16] have shown that there is a good correlation between $1/Q$ and the grain size for both eutectic- and peritectic-forming solutes in Al alloys even though it is an approximation.[15,17–21] Furthermore, it has been shown that the as-cast grain size of other alloys such as magnesium[23] and titanium[24] also correlates well with $1/Q$. Nevertheless, there are still a number of experimental observations that cannot be fully explained by the two concepts of inoculant and solute effects. For example, even under the condition of the same Q values, addition of Ti into pure Al produces significant grain

FENG WANG, Postdoctoral Research Fellow, formerly with the School of Mechanical and Mining Engineering, The University of Queensland, Brisbane, QLD 4072, Australia, is now with the Brunel Centre for Advanced Solidification Technology, Brunel University, Uxbridge, Middlesex UB8 3PH, U.K. ZHI-LIN LIU, Ph.D. Candidate, DONG QIU, Research Fellow, JOHN A. TAYLOR, Associate Professor, and MING-XING ZHANG, Professor, are with the School of Mechanical and Mining Engineering, The University of Queensland. Contact e-mail: mingxing.zhang@uq.edu.au MARK A. EASTON, Professor, formerly with the School of Materials Science and Engineering, Monash University, Clayton, VIC 3800, Australia, is now with School of Aerospace Mechanical and Manufacturing Engineering, RMIT University, Bundoora, VIC 3083, Australia.
Manuscript submitted December 1, 2013.

refinement while addition of eutectic-forming solutes, such as Si, Mg, and Cu, have little grain refining ability when nuclean particles are not deliberately added.[8,21] In fact, understanding the extremely high grain refining efficacy of Ti at addition levels below the maximum solubility has been a long-standing issue of debate.[1–9] Hence, it is considered that there could be an as yet unidentified factor that governs the grain refinement of cast Al alloys.

Solute has been shown to reduce grain size through the development of constitutional supercooling (CS), restricting grain growth, and facilitating subsequent nucleation.[13–15] However, it is unclear whether solute also influences the driving force for solidification, which is essentially the Gibbs free energy difference between the solid and liquid at a given temperature. Normally, the driving force for solidification (including nucleation and growth) is considered as an 'undercooling' or a reduction in temperature below the equilibrium melting temperature as it is assumed that the free energy difference is proportional to the undercooling.[25] However, at a given temperature, as the free energy of alloys is also a function of chemical composition, the free energy difference, i.e., the driving force for solidification, should also depend on the solute concentration in alloys. This implies that Al alloys with different solute additions may have a different driving force for solidification for a given undercooling. As a result, it may lead to a difference in the as-cast grain size. With the advent of more sophisticated Gibbs free energy functions and their accessibility through computational thermodynamics packages, the present work aims to investigate the effect of solute additions on the driving force for solidification, and then to reveal the underlying factor that governs or considerably affects the nucleation and growth during solidification of Al alloys and therefore lead to different as-cast grain sizes.

II. THERMODYNAMIC MODELING DESCRIPTIONS

The progress in development of thermodynamic modeling and the availability of CALPHAD (Computer Coupling of Phase Diagrams and Thermochemistry) in recent years enables the calculation of the free energy difference between liquid and solid of Al alloys.[26,27] As a powerful tool, the commercial software Thermo-Calc[28] has been used to calculate the free energy difference in the present study. Seven solute elements including three eutectic-forming solutes (Cu, Mg, and Si) and four peritectic-forming solutes (Ti, V, Zr, and Nb) are selected to form Al binary alloys, i.e., Al-Cu, Al-Mg, Al-Si, Al-Ti, Al-V, Al-Zr, and Al-Nb. The thermodynamic data sets have been carefully selected from the published literature.[29–41] The data related to the Gibbs energy of each phase were calculated via the CALPHAD method, in which thermodynamic data and related phase equilibria information were used to generate a small set of coefficients for each phase in the system by a least squares optimisation process.[26,27]

It is important to note that, since the present work is only concerned with the Gibbs free energy difference between primary α-Al and the liquid phase, only the thermodynamic data sets for these phases were adopted. As discussed in the following section, it is also reasonable to assume that the small addition of solute does not significantly change the interfacial energy between α-Al and liquid. The relevant parameters required for the free energy difference calculation of these seven systems are listed in Table I.

The Gibbs free energy function, $G_i^{0,\phi}(T) = G_i^{\phi}(T) - H_i^{SER}$, for pure element i (i = Al, Cu, Mg, Si, Ti, V, Zr, and Nb) in any phase is described by an equation of the following form [42]:

$$G_i^{0,\phi}(T) = a + bT + cT\ln T + dT^2 \\ + eT^3 + fT^{-1} + gT^7 + hT^{-9} \quad [1]$$

where H_i^{SER} is the molar enthalpy of the element i at temperature of 298.15 K (25.15 °C) and pressure of 1 bar in its standard element reference state, which is fcc for Al and Cu, hcp for Mg, Ti, and Zr, diamond for Si and bcc for V and Nb. T is the absolute temperature. a, b, c, d, e, f, g, and h are constants. The Gibbs free energy functions for pure Al, Cu, Mg, Si, Ti, V, Zr, and Nb are taken from the Scientific Group Thermodata Europe (SGTE) compilation by Dinsdale.[42]

The Gibbs free energy functions for (α-Al) fcc solid solution and liquid phases are described by the substitutional solution model as follows:

$$G^{\phi} = \sum_i x_i \cdot G_i^{0,\phi} + RT \sum_i x_i \times \ln x_i \\ + \sum_{i,j>i} x_i \times x_j \times \sum_v L_{i,j}^{v,\phi} \times (x_i - x_j)^v \quad [2]$$

where x_i (x_j) represents the mole fraction of element i (j), with i (j) = Al, Cu, Mg, Si, Ti, V, Zr, Nb; R is the gas constant (R = 8.3143 J mol^{-1} K^{-1}) and $L_{i,j}^{v,\phi}$ is the Redlich–Kister parameter representing the interaction between elements i and j as listed in Table I. In Eq. [2], the first and second terms represent the Gibbs free energies for mechanical mixture of elements and ideal mixing, respectively, and the third term corresponds to the excess Gibbs free energy of mixing.

Figure 1 schematically shows the variations of Gibbs free energy (the free energy diagram) of solid and liquid phases with solute concentration at a specified temperature, T_1. It is necessary to mention that, in all the present calculations, the concentrations of solutes are deliberately chosen to ensure that they are all below the maximum solid solubilities of their relevant binary phase diagrams to avoid the complication arising from the formation of eutectic or peritectic structures. This is a reasonable consideration since the solidification of primary α-Al is the major concern when considering grain refinement. The terms x_{el} and x_{es} are the equilibrium concentrations of liquid and solid at T_1. They correspond to the common tangent points L and S on the liquid and solid free energy curves in Figure 1.

It is noteworthy that two different terms have been proposed to define the driving force for solidification in

Table I. Thermodynamic Parameters Used for the Calculation of Solidification Driving Force (Free Energy Difference Between Solid and Liquid) in the Seven Al Binary Systems[29–41]

Phase Name	Model Constituents	Parameters (J/mol formula)
Liquid	(Al, Cu)	$L_{Al,Cu}^{0,Liquid} = -66622 + 8.1T$
		$L_{Al,Cu}^{1,Liquid} = +46800 - 90.8T + 10T\ln T$
		$L_{Al,Cu}^{2,Liquid} = -2812$
(α-Al) FCC	(Al, Cu)	$L_{Al,Cu}^{0,FCC} = -53520 + 2T$
		$L_{Al,Cu}^{1,FCC} = +38590 - 2T$
		$L_{Al,Cu}^{2,FCC} = +1170$
Liquid	(Al, Mg)	$L_{Al,Mg}^{0,Liquid} = -12000 + 8.566T$
		$L_{Al,Mg}^{1,Liquid} = +1894 - 3T$
		$L_{Al,Mg}^{2,Liquid} = +2000$
(α-Al) FCC	(Al, Mg)	$L_{Al,Mg}^{0,FCC} = 4971 - 3.5T$
		$L_{Al,Mg}^{1,FCC} = +900 + 0.423T$
		$L_{Al,Mg}^{2,FCC} = +950$
Liquid	(Al, Si)	$L_{Al,Si}^{0,Liquid} = -11340.1 - 1.23394T$
		$L_{Al,Si}^{1,Liquid} = -3530.93 + 1.35993T$
		$L_{Al,Si}^{2,Liquid} = +2265.39$
(α-Al) FCC	(Al, Si)	$L_{Al,Si}^{0,FCC} = -3143.78 + 0.39297T$
Liquid	(Al, Ti)	$L_{Al,Ti}^{0,Liquid} = -108250 + 38T$
		$L_{Al,Ti}^{1,Liquid} = -6000 + 5T$
		$L_{Al,Ti}^{2,Liquid} = +15000$
(α-Al) FCC	(Al, Ti)	$L_{Al,Mg}^{0,FCC} = -128970 + 39T$
		$L_{Al,Mg}^{1,FCC} = -5000$
		$L_{Al,Mg}^{2,FCC} = +20000$
Liquid	(Al, V)	$L_{Al,V}^{0,Liquid} = -50725 + 9T$
		$L_{Al,V}^{1,Liquid} = -15000 + 8T$
(α-Al) FCC	(Al, V)	$L_{Al,V}^{0,FCC} = -69800 + 15T$
		$L_{Al,V}^{1,FCC} = -8000$
Liquid	(Al, Zr)	$L_{Al,Zr}^{0,Liquid} = -125000 + 35T$
		$L_{Al,Zr}^{1,Liquid} = -10000 + 5.57T$
		$L_{Al,Zr}^{2,Liquid} = +15750$
(α-Al) FCC	(Al, Zr)	$L_{Al,Zr}^{0,FCC} = -120000 + 30T$
		$L_{Al,Zr}^{1,FCC} = -10000$
		$L_{Al,Zr}^{2,FCC} = +15000$

Table I. continued

Phase Name	Model Constituents	Parameters (J/mol formula)
Liquid	(Al, Nb)	$L_{Al,Nb}^{0,Liquid} = -91000 + 25T$
		$L_{Al,Nb}^{1,Liquid} = +6000$
		$L_{Al,Nb}^{2,Liquid} = +15000$
(α-Al) FCC	(Al, Nb)	$L_{Al,Nb}^{0,FCC} = -113500 + 21.1T$
		$L_{Al,Nb}^{1,FCC} = +5000$
		$L_{Al,Nb}^{2,FCC} = +10000$

L is the Redlich–Kister parameter representing the interaction between elements i and j as described in the following section.
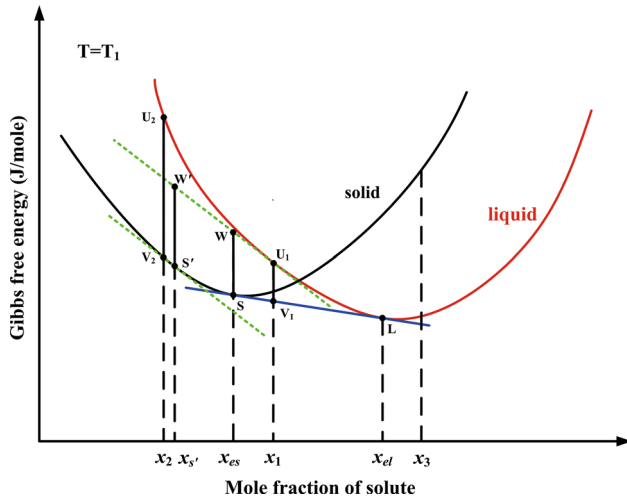

Fig. 1—Schematic graph of the free energy vs mole fraction of solute for liquid and solid phases. The equilibrium free energy change per mole for solidification of liquid of concentration x_1 is U_1 V_1 and that for concentration x_2 is U_2V_2. The driving forces for nucleation of solid of concentrations x_{es} and x_s, from liquid of concentration x_1 are WS and $W'S'$ respectively.[1]

the literature and textbooks.[43–48] Taking a liquid alloy with composition x_1 as an example, its molar free energy is represented by the point U_1 at temperature T_1. For this liquid alloy to solidify at this temperature under equilibrium conditions, it becomes a mixture of a solid solution with composition x_{es} and a liquid solution with composition x_{el}. The overall free energy of this mixed system is represented by the point V_1 on the common tangent line. Therefore, the difference in free energy before and after the completion of the solidification at T_1 is given by U_1V_1 as shown in Figure 1. This is the net driving force for the partial solidification to occur for concentration x_1 at T_1 temperature.

Other researchers[46–48] have suggested that the driving force for solidification process is more accurately defined as the nucleation driving force for the formation of the initial solid. It is assumed that a very small amount of solid will be formed from a local composition of the liquid of essentially the same composition. Therefore, all possible compositions of a solid nucleus, in equilibrium with the liquid of composition x_1, falls along the U_1W' line, which

is the tangent to the liquid free energy curve at point U_1. Thus, the most likely nucleation event is the one that is driven by the largest decrease in free energy. The composition of this solid nucleus corresponds to a point (S' in Figure 1) where the tangent to the solid free energy curve is algebraically equal to the tangent to the free energy curve of the liquid at point U_1. The graphic construction of the driving force for nucleation is illustrated in Figure 1. It can be seen that the driving force for initial nucleation of solid with composition x'_s from the liquid with composition x_1 is $W'S'$.

According to fundamentals of thermodynamics, at a given temperature, the free energy difference between the final state and initial state acts as the driving force for the phase transformation.[43–45] Hence, during solidification, at a particular temperature, the free energy difference between solid and liquid or a mixture of solid and liquid is the driving force for solidification. It should be noted that this driving force is for the whole process of solidification, $i.e.$, nucleation and growth. Generally, higher driving force leads to higher nucleation rate and also higher growth rate. Thus, in the present work, such free energy difference between solid and liquid/or mixture of liquid and solid at any given temperatures is called solidification driving force, which differs from the nucleation driving force defined by other researchers, $W'S'$.[46–48] Therefore, the term, driving force for solidification in the present work means the free energy difference between the initial state which is fully liquid and the final state with an equilibrium mixture of solid and liquid. At temperature T_1, as shown in Figure 1, it is U_1V_1.

As it can be seen from Figure 1, if the solute concentration ($e.g.$, x_3) is above the equilibrium concentration of liquid phase, x_{el}, the Gibbs free energy of liquid is lower than that of the solid solution. In this case, the stable state is liquid and hence the driving force for solidification is zero. When the solute concentration ($e.g.$, x_1) is within the range between the equilibrium concentration of solid solution, x_{es}, and the equilibrium concentration of liquid phase, x_{el}, the stable state is a mixture of liquid and solid as mentioned above. In this case, solidification occurs partially and the Gibbs free energy difference, ΔG ($i.e.$, U_1V_1), can be calculated using the equation:

$$\Delta G = G^s_{x_{es}} \cdot \left(\frac{x_{el} - x_1}{x_{el} - x_{es}} \right) + G^l_{x_{el}} \times \left(\frac{x_1 - x_{es}}{x_{el} - x_{es}} \right) - G^l_{x_1} \quad [3]$$

If the solute concentration (e.g., x_2) is less than the equilibrium concentration of solid solution, x_{es}, the Gibbs free energy of the solid solution is lower than that of the liquid phase and therefore the stable state is fully solid. Thus, the Gibbs free energy difference (i.e., U_2V_2) equals to

$$\Delta G = G^s_{x_2} - G^l_{x_2} \quad [4]$$

Using Eqs. [3] and [4], the variation of Gibbs free energy difference, ΔG, with undercooling, ΔT, can be calculated for the seven alloy systems. In the calculation, $\Delta T = T_l - T$, where T_l is the liquidus temperature that varies with the solute species and concentration and T is the melt temperature.

III. RESULTS AND DISCUSSION

The variation of the free energy difference, ΔG, with undercooling, ΔT, for eutectic and peritectic binary Al alloys at different solute concentrations is shown in Figures 2 and 3, respectively. It is observed that the absolute values of $|\Delta G|$ for all seven alloy systems are always lower than that for pure Al and decrease as the concentrations increase for a particular undercooling. This indicates that addition of solute into pure Al reduces the solidification driving force for a given undercooling. The larger values of $|\Delta G|$, i.e., a larger driving force for solidification, can simultaneously promote both nucleation and growth. Therefore in pure Al, where no constitutional supercooling (CS) forms during solidification due to the absence of solute, once α-Al grains nucleate, they grow rapidly as a result of the large driving force without any growth restriction effect imposed by solute segregation. Hence, coarse columnar grains are normally observed in pure Al. In contrast, the addition of solutes into pure Al induces solute segregation during solidification, resulting in the formation of a CS zone ahead of the growing liquid/solid interface. Considerable research work[13–15] has verified that not

only can such solute segregation restrict the growth of the existing grains, but also that subsequent nucleation can occur within the CS zone, which further impedes the grain growth.

Whilst increased constitutional supercooling greatly reduces the grain size in cast Al alloys through the Q value, the effect that the solute has on the driving force appears to also be important, particularly when effective nucleants are not present. Previous experimental results[21] show that, at the same Q value, the grain refining efficiency varies with solute as illustrated in Figure 4. Peritectic-forming solute Ti at addition levels far below its maximum solubility has significantly higher grain refining efficiency than the other solute, which is supported by previous results in the literature.[3–5,11,49] However, other solute (including Cu, Mg, Si, V, Zr, and Nb) at addition levels below their maximum solubilities in Al, even at a Q value of 12 K (-261 °C) (e.g. Figure 4(d)), have very limited grain refining efficiency in cast Al alloys without inoculation.

In order to fully understand and explain such experimental phenomena, ΔG is replotted against undercooling, ΔT, for similar Q values for all the seven solutes in Figure 5. The same four Q levels as shown in Figure 4 (i.e., 1, 2, 5, and 12) are used. It can be seen that at each Q level, the values of $|\Delta G|$ differ between solutes. At $Q \approx 1$ (Figure 5a), the $|\Delta G|$ values of Cu, Si, and Mg are slightly smaller than V and Nb, which are in turn smaller than Zr and Ti. Note that the maximum Q value obtainable by Zr and Nb is around 1 K (-272 °C) due to their very small maximum solubilities (0.11 wt pct Zr and 0.15 wt pct Nb) in solid Al. The very small growth restriction effect of Zr and Nb dominates their grain refining efficiencies at concentrations below the maximum solubilities in Al even though these two alloys have large driving force for solidification for a given undercooling.[50,51] This is quite similar to the case of pure Al as discussed above. With an increase in Q value (Figures 5(b), (c)), the difference in $|\Delta G|$ values between eutectic-forming solutes, Cu, Si, and Mg, and peritectic-forming solutes, Ti and V, increases. At $Q \approx 12$ (Figure 5(d)), the $|\Delta G|$ values of Cu and Mg are significantly smaller than that of Ti for a given undercooling. Therefore, Figures 5(a) through (d) show that the driving force for solidification generally increases as CS increases for all solute elements. However, different
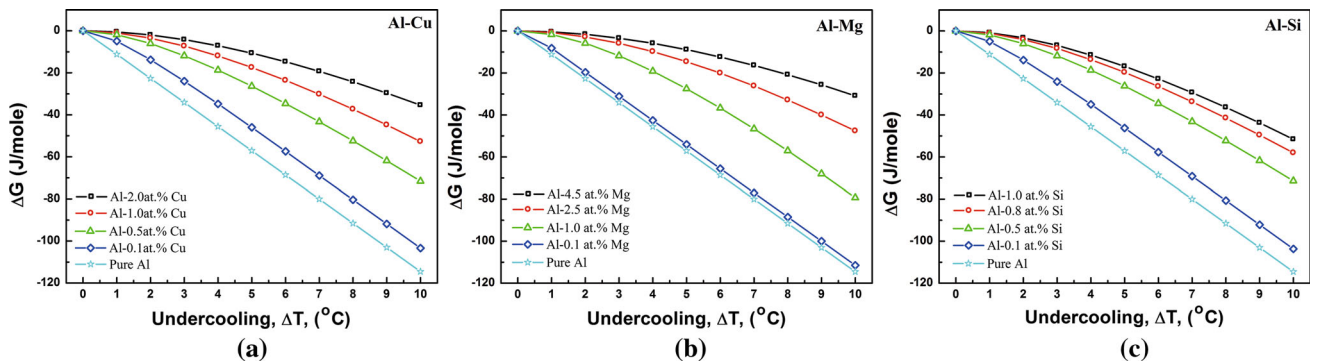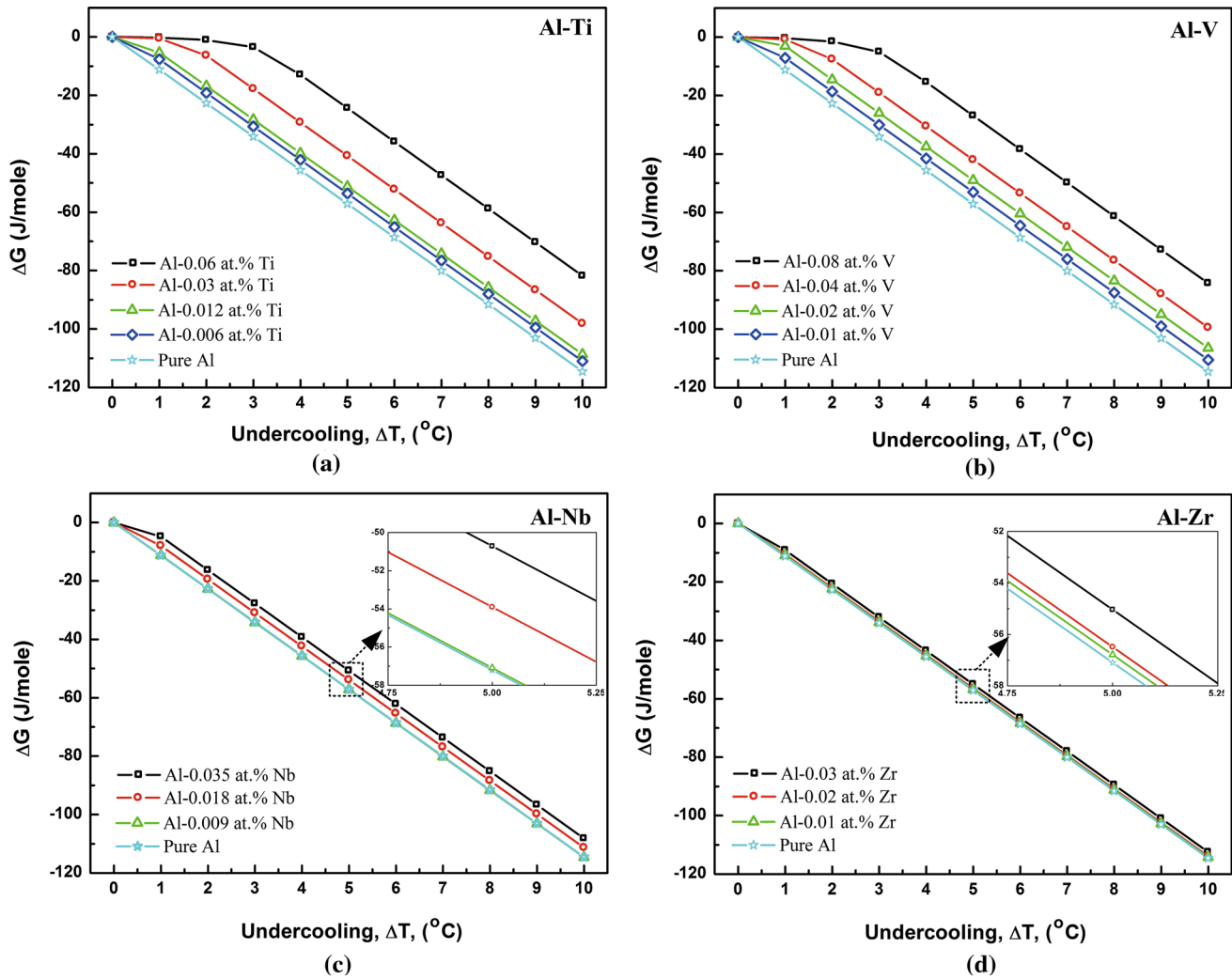

Fig. 2—Calculated variation of the Gibbs free energy difference, ΔG, with undercooling, ΔT, at different solute contents (at. pct) in (a) Al-Cu, (b) Al-Mg and (c) Al-Si alloys.

Fig. 3—Calculated variation of the Gibbs free energy difference, ΔG, with undercooling, ΔT, at different solute contents (at. pct) in (a) Al-Ti, (b) Al-V, (c) Al-Nb and (d) Al-Zr alloys.

solute elements provide different driving forces, *i.e.*, peritectic-forming solutes provide larger driving force than eutectic-forming solutes at a given Q value. It is suggested that the higher grain refining efficiency through adding peritectic-forming alloying elements, in particular Ti, is attributed to the larger solidification driving force associated with this type of alloy, because the higher driving force leads to higher nucleation rate. As adding Ti into Al results in the largest solidification driving force, as shown in Figure 4, Ti has the highest grain refining efficiency in Al of all the 7 alloying elements. However, one may argue that the higher solidification driving force also leads to higher growth rate, which tends to coarsen the grains. In fact, the interaction between grain nucleation and growth during solidification has been well described by the newly developed interdependence theory of grain refinement.[14]

According to the interdependence theory,[14] the growth of an existing grain leads to the development of CS which can promote subsequent nucleation within the CS zone. Once the CS is high enough to provide sufficient driving force to trigger nucleation of another grain, the growth of the existing grain will be limited. Growth of such new grains will generate further CS, which in turn promotes repeating nucleation within the CS zones. It is necessary to mention that, under ideal situations, the total supercooling in the liquid ahead of the growing solid/liquid interface is the sum of both CS and thermal supercooling where the thermal undercooling is determined by the temperature gradient in the melt. However, in most practical situations of a solidifying melt, the contribution of thermal undercooling is small compared with the CS in the bulk of the melt. As a result, it is generally acknowledged that CS makes the dominant contribution to supercooling in the liquid ahead of the advancing solid/liquid interface.[13–16] StJohn and his co-workers[14] proposed that the average gain size is determined by three components as illustrated in Figure 6 and given by Eq. [5][14]:
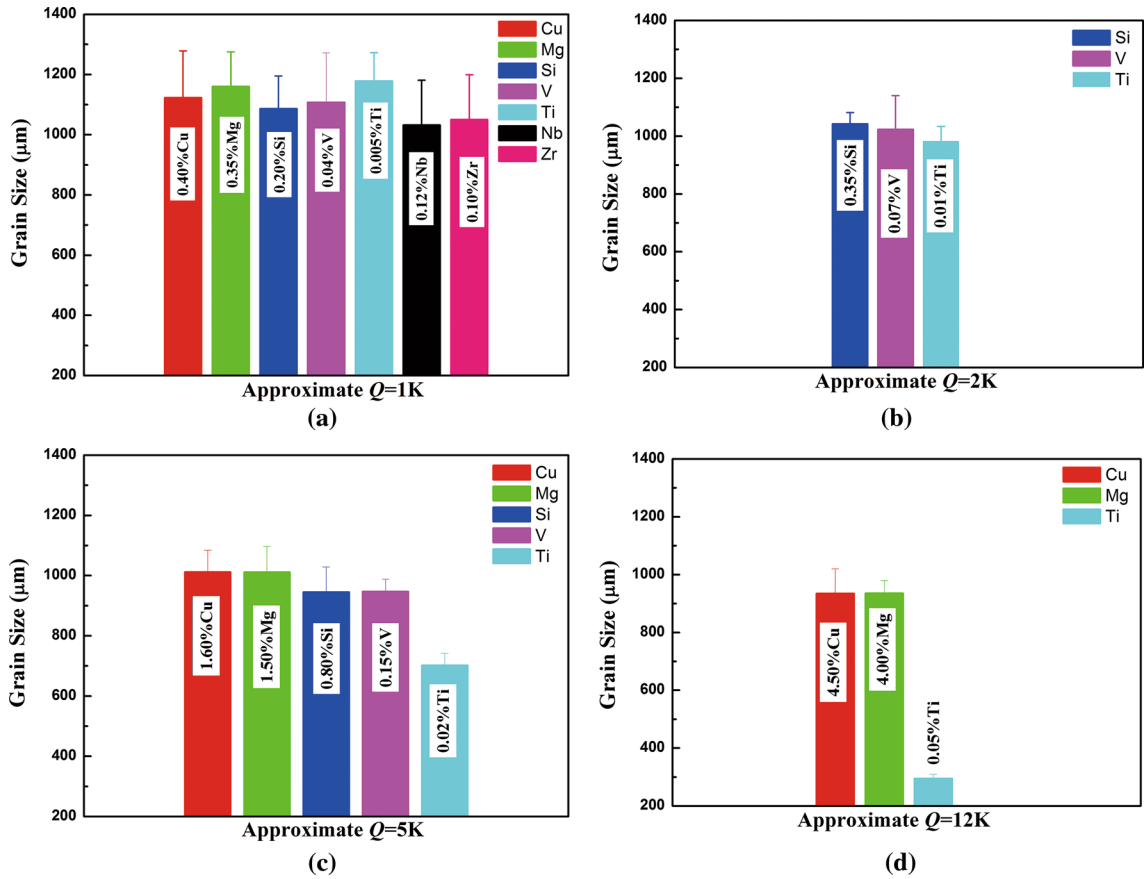
Fig. 4—Average grain sizes of various Al alloys with growth restriction factor, Q, at addition levels below their maximum solubilities in Al: (a) Approx. Q = 1 K (−272 °C), (b) Approx. Q = 2 K (−271 °C), (c) Approx. Q = 5 K (−268 °C), (d) Approx. Q = 12 K (−261 °C).[21]

$$d_{gs} = \frac{D \times z \times \Delta T_n}{vQ} + \frac{4.6 \times D}{v} \times \left(\frac{c_l^* - c_0}{c_l^*(1 - k)} \right) + x_{sd} \quad [5]$$

where D is the diffusion coefficient, v the growth rate, $z \cdot \Delta T_n$ the CS required to re-establish the necessary CS to provide sufficient driving force for activating further nucleation, c_l^* the solute composition in the liquid at the solid/liquid interface, and c_0 is the original composition of the liquid alloy, x_{sd} is the distance between the most potent available nucleant particles. The details of the derivation and formulation of the interdependence theory, in particular the concentration profile of the CS zone are available in the references.[13,14] When no inoculant particles are deliberately added in the alloy, the third component, x_{sd}, represents the mean distance between the most potent native nucleant particles naturally occurring in the alloy. Thus, it is reasonable to assume that the value of x_{sd} for native particles and the driving force required to facilitate the subsequent nucleation on the native particles would be similar for the same base alloys.

In this case, the average grain size, d_{gs}, is therefore determined by the sum of the first two components. As shown in Figure 6, the first two components x_{cs} and x'_{dl} together represent a nucleation-free zone, x_{nfz}, where the driving force generated by the CS is always less than that required for initiating new grains on the most potent

particles within the distribution. It is noted, from Eq. [5] that, under the same casting condition, x_{nfz}, i.e., the length of the nucleation-free zone, is proportional to x_{cs}, i.e., the minimum distance required to generate necessary CS, which is determined by the driving force required for triggering further nucleation on the most potent available nucleant particle. Therefore, the average grain size, d_{gs}, of alloys without deliberate addition of inoculants is mainly determined by the value of x_{cs}, i.e., the minimum distance required to generate necessary CS to provide sufficient driving force for a nucleation event to occur ahead of the interface.

Based on the above discussion in terms of the interdependence theory, it is deduced that, to overcome the solidification barrier, peritectic alloys require smaller CS to provide the necessary driving force to activate subsequent nucleation, because for a given undercooling peritectic alloys have significantly larger driving force (Figure 5). This implies that, compared with addition of eutectic-forming solutes, addition of peritectic-forming solutes can quickly build up the required CS zone for the subsequent nucleation on the native nucleant particles, corresponding to smaller value of x_{cs}. This limits the growth of the existing grain. As a result, adding peritectic-forming solutes produces a finer grain size. In comparison to peritectic-forming solutes Zr and Nb, addition of Ti is not only associated with a large
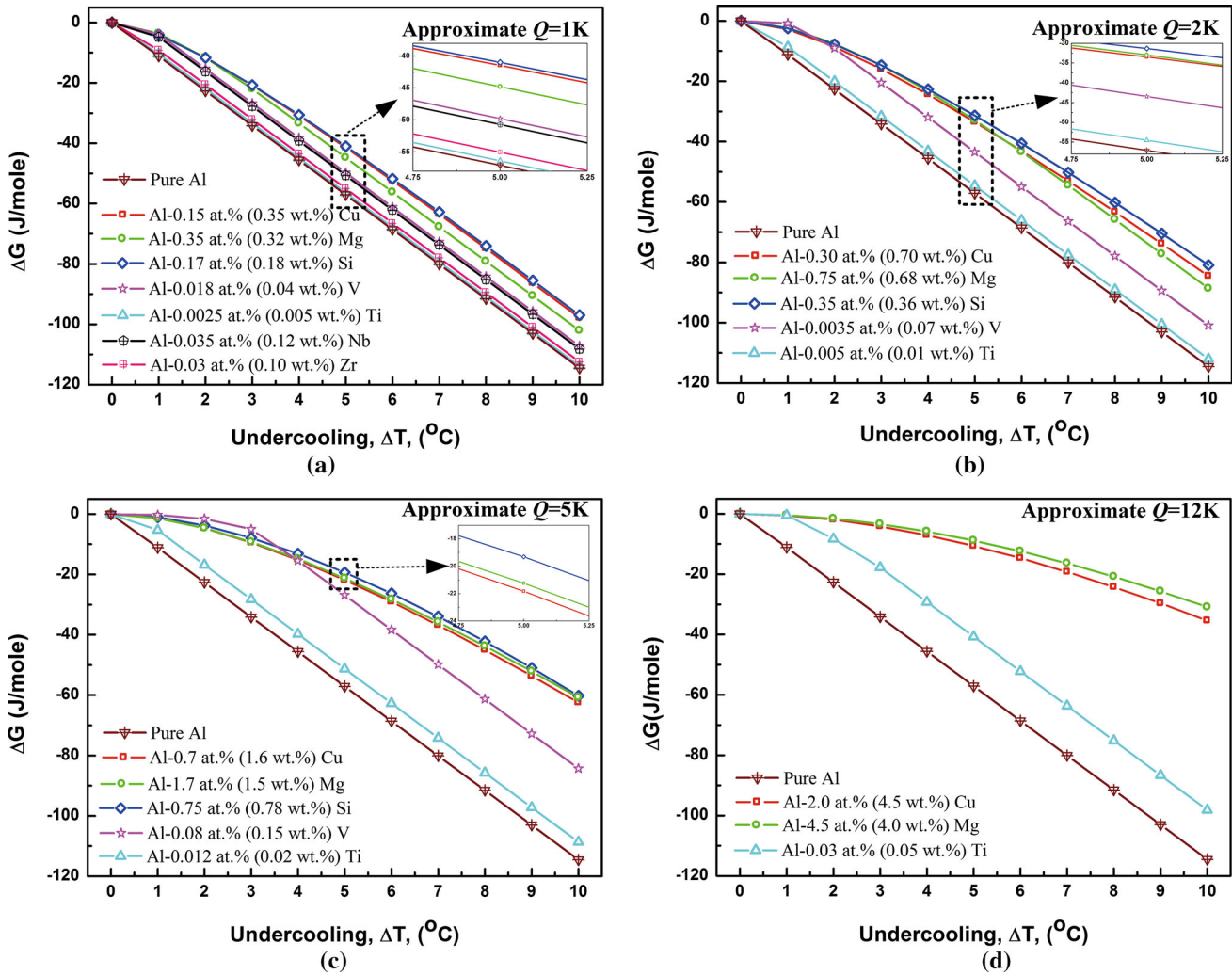
Fig. 5—Calculated values of the Gibbs energy difference, ΔG, as a function of undercooling, ΔT [0 K to 10 K (-273 °C to -263 °C)], with various solutes for four different Q levels (*a*) Approx. $Q = 1$ K (-272 °C), (*b*) Approx. $Q = 2$ K (-271 °C), (*c*) Approx. $Q = 5$ K (-268 °C) and (*d*) Approx. $Q = 12$ K (-261 °C).
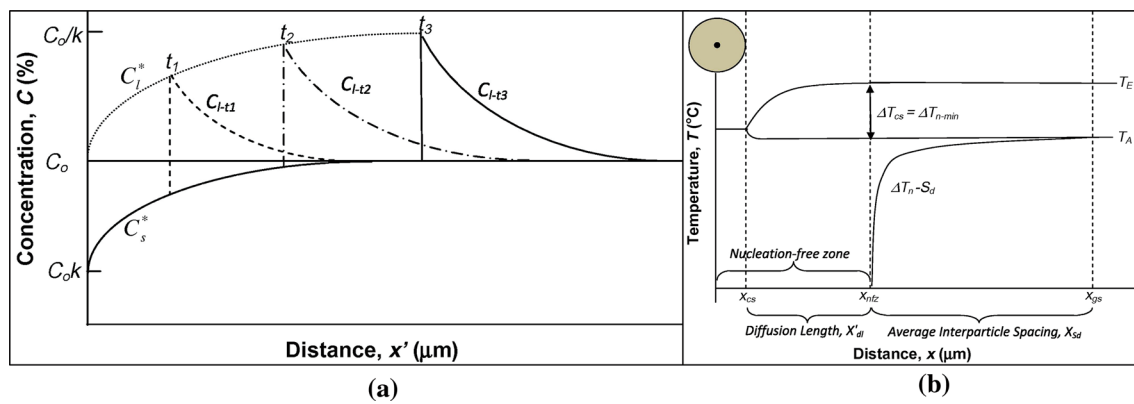

Fig. 6—(*a*) Development of the solute concentration profiles in the liquid ahead of a planar advancing front moving from left to right; (*b*) A representation showing the three components that together compose the grain size of the microstructure: x_{cs}, x'_{dl} and x_{sd}. The first component, x_{cs}, is the minimum growth distance required to generate sufficient driving force for triggering further nucleation; the second component, x'_{dl}, is the associated diffusion length with the growth distance x_{cs}; and the last component, x_{sd}, is the spatial mean distance to the most potent available nucleant particles.[14]

Table II.   Solid–Liquid Interface Energies for the Binary Al Alloys[55–59]

System	Solid Phase	Liquid Phase	Solid–Liquid Interface Energy $\sigma_{SL} \times 10^{-3}$ (J m^{-2})
Al	Al	Al	93
			97
			113
			121
			141
Al-Cu	Al	AlCu	163.40 ± 21.20
			160.01 ± 19.20
Al-Mg	Al	AlMg	149.20 ± 19.40
Al-Si	Al	AlSi	168.95 ± 21.90
Al-Ni	Al	AlNi	171.56 ± 20.58
Al-Ag	Al	AlAg	166.32 ± 21.62
Al-Ti	Al	AlTi	174.62 ± 20.95
			170.72 ± 16.22

solidification driving force for a given undercooling but also associated with large available Q value, leading to the smallest grain size. In contrast, to achieve the same driving force required for activation of the subsequent nucleation on the same native nucleant particles, the eutectic-forming solutes need larger CS due to the smaller solidification driving force for a given undercooling as illustrated in Figure 5. This means that the existing grain has a longer time to grow, corresponding to a greater value of x_{cs}.

Hence, the grain sizes in the alloys with addition of eutectic-forming solutes are very coarse. Previous grain size data measured by the authors[21] have shown that the grain size for Al-0.05Ti ($\approx$295 μm) is much smaller than those for Al-4.5Cu ($\approx$925 μm) and Al-4.0Mg ($\approx$945 μm) alloys, despite having similar Q values [$\approx$12 K (-261 °C)]. In addition, Easton and StJohn[8] have also obtained similar results, *i.e.*, Al-0.05Ti [$Q \approx 12$ K (-261 °C)] has a grain size of around 223 μm while Al-2.0Si [$Q \approx 12$ K (-261 °C)] has a much larger grain size ($\approx$837 μm). Furthermore, it is found that, in the work of Spittle and Sadli[52] who used a completely different casting procedure (the Alcan test), the grain size of Al-0.01Ti [$Q \approx 2.2$ K (-270.8 °C)] has a much smaller grain size ($\approx$1200 μm) than the grain size ($\approx$1858 μm) for Al-0.35Si [$Q \approx 2.1$ K (-270.9 °C)] alloy. These experimental results agree well with the above discussion.

It may be argued that the interfacial energy between solid and liquid plays an important role in solidification because the interfacial energy is one of the major nucleation barriers. Generally, the solid–liquid interface energy varies with addition of solutes into pure metals.[53,54] In Al alloys, the interfacial energies between solid α-Al and various binary alloy melts have been experimentally determined previously. They are listed in Table II.[55–59] It is noted that the variation of the solid–liquid interface energy, σ_{SL}, resulted from solutes addition, is in the order of 10^{-2} J m^{-2}. The unit of J mol^{-1} for ΔG used in the present work in Figures 2, 3 and 5 can be converted to J m^{-3} through dividing the ΔG values by molar volume of solid solution, which is within the range of $8.8 \sim 11.6 \times 10^{-6}$ m^3 mol^{-1}.[55–59] It is found that the variation of present $|\Delta G|$ values incurred by solute addition is in the order of

10^4~10^5 J m^{-3} (10^3~10^4 J m^{-2}). This is significantly larger than the variation of σ_{SL}. Therefore, the assumption in the present work to ignore the effect of different solutes on the solid–liquid interface energy is justified.

Combining the present thermodynamic calculations with previous experiment results,[21] it is concluded that the grain refinement of cast Al alloys is affected by heterogeneous nucleation, growth restriction factor, and the thermodynamic driving force. Peritectic systems are particularly favorable as they tend to have all of these factors which appears to be why peritectic systems are such effective grain refining systems. No single factor can define the grain refining efficiency. To be an effective grain refiner, solute added into the Al melt must fulfill the following three criteria: (1) the solute must lead to large constitutional supercooling, which is expressed by large growth restriction factor, Q; (2) the solute must provide large solidification driving force, $|\Delta G|$ for a given Q, which are best achieved by the solute being peritectic-forming, which have the added benefit of providing a pro-peritectic phase as an *in situ* nucleant particle. The role of peritectics on grain refinement of cast Al alloys has been discussed in more details in References 21, 50, 51 and the growth restriction factor has been considerably studied previously.[16,19–22]

The present work has introduced the effect of the addition of solute on the free energy difference between solid and liquid and proposes it has a significant effect on grain refinement. Combined with the concept of constitutional supercooling, this thermodynamic factor provides a more reasonable solution to some long-standing problems. For example, previous experimental results[8,21] have shown that addition of Ti generally produces more significant grain refinement of Al alloys than additions of other solutes even though the same Q value is achieved. Such high grain refining efficiency of Ti was previously considered as a result of the formation of unknown nucleant particles due to the high reactivity of Ti with impurities.[21] This assumption has never been experimentally proved. However, the present work provides an alternative explanation using thermodynamics. As illustrated in Figure 5, for the same Q value, Ti solute has a relatively large driving force for solidification in Al compared to other solute. This leads

to a reduced CS requirement, which corresponds to a shorter distance of growth being required to sufficiently activate the subsequent nucleation within the CS zone, leading to significant grain refinement. This is probably responsible for the high grain refining efficiency of Ti in cast Al alloys compared with other solutes added at levels to provide a similar Q value.

IV. CONCLUSIONS

The variation of driving force for solidification (*i.e.*, $|\Delta G|$) with undercooling, ΔT, has been calculated at different solute additions and Q values for both eutectic and peritectic Al binary alloys. The calculation leads to the following conclusions:

1. The solidification driving force, $|\Delta G|$, for Al alloys is always lower than that for pure Al and decreases with increasing solute content for a given undercooling. However, addition of solute into Al leads to the formation of constitutionally undercooled zone ahead of the solid/liquid interface, which in turn significantly reduces the grain growth and facilitates further nucleation.
2. At the same level of Q value and undercooling, the solidification driving force of peritectic Al alloys is greater than that of the eutectic Al alloys. The larger solidification driving force of peritectic alloys not only promotes the initial nucleation in the liquid metal, but also facilitates subsequent nucleation within the CS zone. The latter will also constrain the growth of the existing Al grains. Thus, compared with the eutectic alloys, a sufficient CS zone for subsequent nucleation can be created at a smaller x_{cs} value in peritectic alloys, resulting in finer grains.
3. Within the seven solutes investigated, addition of Ti retains the largest solidification driving force and highest available Q value, which significantly promotes the initial nucleation in the liquid, and the subsequent nucleation within the CS zone. Therefore, sufficient CS zone to facilitate subsequent nucleation can be developed with less growth of the existing grain, leading to effective grain refinement. Thus, Ti has the highest grain refining efficiency in Al alloys relative to other solutes.
4. It is considered that the grain refinement of cast metals, at least for Al alloys, is governed by the combined effect of heterogeneous nucleation, the growth restriction factor, and thermodynamic driving force for solidification, $|\Delta G|$.

REFERENCES

1. B.S. Murty, S.A. Kori, and M. Chakraborty: *Inter. Mater. Rev.*, 2002, vol. 47, pp. 3–29.
2. T.E. Quested: *Mater. Sci. Technol.*, 2004, vol. 20, pp. 1357–69.
3. A. Cibula: *J. Inst. Met.*, 1951, vol. 80, pp. 1–16.
4. D.G. McCartney: *Inter. Mater. Rev.*, 1989, vol. 34, pp. 247–60.
5. M.M. Guzowski, G.K. Sigworth, and D.A. Sentner: *Metall. Trans. A*, 1987, vol. 18A, pp. 603–19.
6. P.S. Mohanty and J.E. Gruzleski: *Acta Metall. Mater.*, 1995, vol. 43, pp. 2001–12.
7. M.A. Easton and D.H. StJohn: *Metall. Mater. Trans. A*, 1999, vol. 30A, pp. 1613–23.
8. M.A. Easton and D.H. StJohn: *Metall. Mater. Trans. A*, 1999, vol. 30A, pp. 1625–33.
9. A.L. Greer, P.S. Cooper, M.W. Meredith, W. Schneider, P. Schumacher, J.A. Spittle, and A. Tronche: *Adv. Eng. Mater.*, 2003, vol. 5, pp. 81–91.
10. M. Johnsson, L. Backerud, and G.K. Sigworth: *Metall. Trans. A*, 1993, vol. 24A, pp. 481–91.
11. J.A. Marcantonio and L.F. Mondolfo: *Metall. Trans.*, 1971, vol. 2, pp. 465–71.
12. P. Schumacher and A.L. Greer: *Eighth International Conference on Rapidly Quenched and Metastable Materials*, 22–27 Aug, 1993, vol. A181–A182, Switzerland, 1994, pp. 1335–39.
13. M.A. Easton and D.H. StJohn: *Acta Mater.*, 2001, vol. 49, pp. 1867–78.
14. D.H. StJohn, M. Qian, M.A. Easton, and P. Cao: *Acta Mater.*, 2011, vol. 59, pp. 4907–21.
15. M. Johnsson: *Thermochim. Acta*, 1995, vol. 256, pp. 107–21.
16. M. Qian, P. Cao, M.A. Easton, S.D. McDonald, and D.H. StJohn: *Acta Mater.*, 2010, vol. 58, pp. 3262–70.
17. I. Maxwell and A. Hellawell: *Acta Metall.*, 1975, vol. 23, pp. 229–37.
18. M. Johnsson and L. Baeckerud: *Z. Metallkd.*, 1996, vol. 87, pp. 216–20.
19. M.A. Easton and D.H. StJohn: *Metall. Mater. Trans. A*, 2005, vol. 36A, pp. 1911–20.
20. M.A. Easton and D.H. StJohn: *Mater. Sci. Eng. A*, 2008, vol. 486, pp. 8–13.
21. F. Wang, Z. Liu, D. Qiu, J.A. Taylor, M.A. Easton, and M.-X. Zhang: *Acta Mater.*, 2013, vol. 61, pp. 360–70.
22. D.H. StJohn, P. Cao, M. Qian, and M.A. Easton: *Adv. Eng. Mater.*, 2007, vol. 9, pp. 739–46.
23. D.H. StJohn, Q. Ma, M.A. Easton, C. Peng, and Z. Hildebrand: *Metall. Mater. Trans. A*, 2005, vol. 36A, pp. 1669–79.
24. M.J. Bermingham, S.D. McDonald, M.S. Dargusch, and D.H. St.John: *J. Mater. Res.*, 2008, vol. 23, pp. 97–104.
25. J.H. Perepezko and W.S. Tong: *Nucleation Control*, Royal Society, Cambridge, 2003, pp. 447–61.
26. H.L. Lukas, S.G. Fries, and B. Sundman: *Computation Thermodynamics (The CALPHD Method)*, Cambridge University Press, New York, 2007.
27. N. Saunders and A.P. Miodownik: *CALPHAD (Calculation of Phase Diagrams): A Comprehensive Guide*, Pergamon, Oxford; New York, 1998.
28. J.O. Andersson, T. Helander, L. Höglund, P. Shi, and B. Sundman: *CALPHAD*, 2002, vol. 26, pp. 273–312.
29. S.L. Chen, Y. Zuo, H. Liang, and Y.A. Chang: *Metall. Mater. Trans. A*, 1997, vol. 28A, pp. 435–46.
30. S.-W. Chen, Y.-Y. Chuang, Y. Austin Chang, and M. Chu: *Metall. Trans. A*, 1991, vol. 22A, pp. 2837–48.
31. N. Saunders: *CALPHAD*, 1990, vol. 14, pp. 61–70.
32. J. Grobner, D. Kevorkov, I. Chumak, and R. Schmid-Fetzer: *Z. Metallkd.*, 2003, vol. 94, pp. 976–82.
33. P. Liang, H.-L. Su, P. Donnadieu, M.G. Harmelin, A. Quivy, P. Ochin, G. Effenberg, H.J. Seifert, H.L. Lukas, and F. Aldinger: *Z. Fuer Metallkunde/Mater. Res. Adv. Tech.*, 1998, vol. 89, pp. 536–40.
34. J. Grobner, H.L. Lukas, and F. Aldinger: *CALPHAD*, 1996, vol. 20, pp. 247–54.
35. H. Feufel, T. Goedecke, H.L. Lukas, and F. Sommer: *J. Alloys Compd.*, 1997, vol. 247, pp. 31–42.
36. U.R. Kattner, J.C. Lin, and Y.A. Chang: *Metall. Trans. A*, 1992, vol. 23A, pp. 2081–90.

37. I. Ohnuma, Y. Fujita, H. Mitsui, K. Ishikawa, R. Kainuma, and K. Ishida: *Acta Mater.*, 2000, vol. 48, pp. 3113–23.
38. V.T. Witusiewicz, A.A. Bondar, U. Hecht, S. Rex, and T.Y. Velikanova: *J. Alloys Compd.*, 2008, vol. 465, pp. 64–77.
39. N. Saunders and V.G. Rivlin: *Mater. Sci. Technol.*, 1986, vol. 2, pp. 521–27.
40. T. Wang, Z. Jin, and J.C. Zhao: *J. Phase Equilibria*, 2001, vol. 22, pp. 544–51.
41. I. Ansara, A.T. Dinsdale, and M.H. Rand, eds.: *COST 507*, European Communities, Belgium, 1998.
42. A.T. Dinsdale: *CALPHAD*, 1991, vol. 15, pp. 317–425.
43. W. Kurz and D.J. Fisher: *Fundamentals of Solidification*, Trans Tech Publications, Switzerland, 1998.
44. D.A. Porter, K. Easterling, and M.Y. Sherif: *Phase Transformations in Metals and Alloys*, CRC Press, Boca Raton, FL, 2009.
45. J.A. Dantzig and M. Rappaz: *Solidification*, EPFL Press, Lausanne, 2009.
46. H. Fredriksson and U. Åkerlind: *Thermodynamic Analysis of Solidification Processes in Metals and Alloys. Solidification and Crystallization Processing in Metals and Alloys*, Wiley, New York, 2012, pp. 42–98.
47. M. Glicksman: *Thermodynamics of Crystal-Melt Phase Change. Principles of Solidification*, Springer, New York, 2011, pp. 27–51.
48. E Clouet: *Modeling of Nucleation Processes. Fundamentals of Modeling for Metals Processing*, ASM International, Brussels, 2009, vol. 22A, pp. 203–19.
49. M.D. Eborall: *J. Inst. Met.*, 1949, vol. 76, pp. 295–320.
50. F. Wang, D. Qiu, Z.-L. Liu, J.A. Taylor, M.A. Easton, and M.-X. Zhang: *Acta Mater.*, 2013, vol. 61, pp. 5636–45.
51. F. Wang, D. Qiu, Z.-L. Liu, J.A. Taylor, M.A. Easton, and M.-X. Zhang: *J. Appl. Crystallogr.*, 2014, vol. 47, pp. 770–79.
52. J.A. Spittle and S. Sadli: *Mater. Sci. Technol.*, 1995, vol. 11, p. 533.
53. N. Eustathopoulos: *Int. Met. Rev.*, 1983, vol. 28, pp. 189–210.
54. L. Battezzati: *RQ10, Tenth International Conference on Rapidly Quenched and Metastable Materials, 23–27 Aug. 1999*, Elsevier, Switzerland, 2001, vol. A304-A306, pp. 103–21.
55. M. Gunduz and J.D. Hunt: *Acta Metall.*, 1985, vol. 33, pp. 1651–72.
56. N. Marasli and J.D. Hunt: *Acta Mater.*, 1996, vol. 44, pp. 1085–96.
57. M. Gunduz and J.D. Hunt: *Acta Metall.*, 1989, vol. 37, pp. 1839–45.
58. K. Keslioglu, M. Gunduz, H. Kaya, and E. Cadirli: *Mater. Lett.*, 2004, vol. 58, pp. 3067–73.
59. S. Engin, U. Boyuk, and N. Marasli: *J. Alloys Compd.*, 2009, vol. 488, pp. 138–43.